Inorganic Chemistry
Article
Cite This: Inorg. Chem. XXXX, XXX, XXX−XXX
pubs.acs.org/IC

Multifunctional Copper(I) Coordination Polymers with Aromatic Mono- and Ditopic Thioamides

Javier Troyano,[†] Eduardo Zapata,[†] Josefina Perles,[‡] Pilar Amo-Ochoa,[†,⊥] Vanesa Fernández-Moreira,[§] José I. Martínez,[∥] Félix Zamora,*[,†,⊥,¶] and Salomé Delgado*[,†,⊥]

[†]Departamento de Química Inorgánica, [‡]Servicio Interdepartamental de Investigación, and [⊥]Institute for Advanced Research in Chemical Sciences, Universidad Autónoma de Madrid, Madrid 28049, Spain

[§]Departamento de Química Inorgánica, Instituto de Síntesis Química y Catálisis Homogénea, CSIC, Universidad de Zaragoza, Zaragoza 50009, Spain

[∥]Departamento de Nanoestructuras, Superficies, Recubrimientos y Astrofísica Molecular, Instituto de Ciencia de Materiales de Madrid, Madrid 28049, Spain

[¶]Instituto Madrileño de Estudios Avanzados en Nanociencia, Cantoblanco, Madrid 28049, Spain

Supporting Information

ABSTRACT: Direct reactions under ambient conditions between CuX (X = Br, I) and thiobenzamide (TBA) were carried out at different ratios, giving rise to the formation of a series of one-dimensional (1D) coordination polymers, (CPs) $[CuI(TBA)]_n$ (**1**), $[Cu_3I_3(TBA)_2]_n$ (**4**), and $[CuBr(TBA)]_n$ (**5**), as well as two molecular complexes, $[CuI(TBA)_3]$ (**2**) and $[Cu_2I_2(TBA)_4]\cdot 2MeCN$ (**3**). Recrystallization of **1** and **5** yielded a series of isostructural 1D CP solvated species, $[CuI(TBA)\cdot S]_n$ (**1**·S; S = tetrahydrofuran, acetone, methanol) and $[CuBr(TBA)\cdot S]_n$ (**5**·S; S = tetrahydrofuran, acetone), respectively. Similar reactions between CuI and 1,4-dithiobenzamide (DTBA) allowed the isolation of a series of two-dimensional (2D) CPs $[CuI(DTBA)\cdot S]_n$ (**6**·S; S = *N*,*N*-dimethylformamide, acetonitrile, methanol). Interestingly, **1**·S and **5**·S showed variable luminescence and electrical semiconductivity depending on the different solvents located in their structures. Thus, **1** and **5** could display potential application for sensing volatile organic vapors by virtue of the significant changes in their emission upon solvent exposure, even by the naked eye. Theoretical calculations have been used to rationalize these electronic properties.

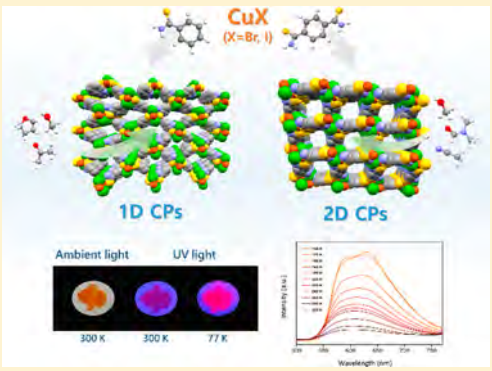

INTRODUCTION

Coordination polymers (CPs) have attracted increasing attention in recent years because of their interesting architectures and physicochemical properties.[1] In particular, those with copper(I) are relevant because of their structural diversity, electrical conductivity,[2] and luminescence properties.[3] Additionally, the development of new systems based on copper(I) is strongly motivated by its low toxicity, low cost, and availability of copper compared to the noble metals and rare earths.[4] Among these systems, copper(I) halides represent a versatile type of building block that has been successfully used for the synthesis of CPs in combination with different neutral ligands and offers appreciable optoelectronic properties.[5] On the other hand, organosulfur-containing ligands have demonstrated their potential as linkers in the synthesis of metal−organic networks showing interesting electrical and luminescence properties.[6]

Although heterocyclic thioamides constitute an important class of sulfur-containing organic compounds that have been largely studied for their interesting chemical, biochemical, structural, and spectroscopic properties,[7] structurally simple thioamides, such as thiobenzamide (TBA) and 1,4-dithiobenzamide (DTBA), have been scarcely developed in the field of supramolecular chemistry.[8] Indeed, thioamides are very versatile ligands in their coordination modes because of the presence of nitrogen and sulfur donor sites. They have the ability to behave as bidentate chelate or bridging ligands or as monodentate "soft" ligands via sulfur coordination or "hard" ligands through a nitrogen site. Thus, in complexes of TBA or DTBA with "soft" ions such as copper(I), those ligands compete with "soft" anions such as the heavier halide ions. Additionally, the hydrogen-bonding interactions of amide groups could play an essential role in the autoassembly process.

Because we have previously established that CPs based on copper(I) with organosulfur ligands are highly desirable to obtain materials with multifunctional properties,[2c,d,9] in this work we have focused on the potential of TBA and DTBA to produce multifunctional materials with electrical conductivity and photoluminescence.

Received: December 3, 2018

DOI: 10.1021/acs.inorgchem.8b03364
Inorg. Chem. XXXX, XXX, XXX−XXX

EXPERIMENTAL SECTION

Materials and Methods. All of the reagents were purchased from Sigma-Aldrich and used as received. The ligand 1,4-dithiobenzamide (DTBA) was prepared by a previously published method.[10] Fourier transform infrared (FT-IR) spectra (KBr pellets) were recorded using a PerkinElmer 1650 spectrophotometer. Carbon, hydrogen, nitrogen, and sulfur elemental analyses were performed by using a PerkinElmer 240 B microanalyzer. Powder X-ray diffraction (PXRD) experiments were carried out using a PANalytical X'Pert Pro diffractometer with a $\theta/2\theta$ primary monochromator and a fast X'Celerator detector. The samples were analyzed by scanning $\theta/2\theta$. Steady-state photoluminescence spectra were recorded on a Jobin-Yvon Horiba Fluorolog FL-3-11 spectrometer using band pathways of 3 nm for both excitation and emission. The phosphorescence lifetimes were recorded with an IBH 5000F coaxial nanosecond flashlamp. The lifetime data were fitted with a Jobin-Yvon software package. Measurements at variable temperature were done with an Oxford Cryostat Optistat DN. The lifetime data were fitted using the Jobin-Yvon IBH software *DAS6*, version 6.1.

X-ray Data Collection and Crystal Structure Determination. Data collection was carried out on a Bruker Kappa Apex II diffractometer, using graphite-monochromated Mo Kα radiation (λ = 0.71073 Å) and operating at 50 kV and 30 mA. The crystal structures of the compounds were determined by single-crystal X-ray diffraction at room temperature (RT), except for the samples with low stability in normal conditions; in particular, the higher-temperature data for **5** were collected at 250 K, and for **5**·acetone and **6** MeCN, only a low-temperature data collection was made (at 200 and 100 K, respectively). Additionally, compounds **1**, **1**·S [S = tetrahydrofuran (THF), acetone, methanol (MeOH)], **5**, **5**·THF, and **6**·DMF (DMF = *N*,*N*-dimethylformamide) were measured at 110 K to observe the influence of low temperature in the solid-state arrangement. Detailed information about the structural determination is collected in Figures S1−S23 and Tables S1−S67.

In the structure of compound **6**·DMF, the atoms in the solvent molecules are not involved in hydrogen bonds in two different positions, and a disorder model was done accordingly (Figure S13).

Direct-Current Electrical Conductivity Determination. Electrical conductivity measurements were performed on different single crystals of **1**·acetone, **1**·MeOH, **4**, **5**·THF, **5**·acetone, and **6**·DMF and in different compact pellets in the case of **1**, **1**·THF, and **5**. In all cases, except for compound **6**·DMF, the two contacts are made with carbon paint at 300 K. The small size of CP **6** crystals only allows two direct contacts with the metal tips (without the carbon paste). The contacts were made with platinum wires (25 μm diameter). The samples were measured at 300 K by applying an electrical current with voltages from +10 to −10 V.

Computational Methods. To analyze the electronic, optical, and excitation properties of the different compounds in the present study, we performed a large battery of first-principles static, time-dependent density functional theory (TDDFT)-based, and single-excitation calculations. A TDDFT formalism was employed to compute the excitation spectra,[11] as implemented in the plane-wave simulation package *QUANTUM ESPRESSO* distribution (http://www.quantum-espresso.org). In the calculations, we used the simulation cells and structures resolved at different temperatures as obtained by X-ray diffraction experiments, yielding residual forces acting on each atom below 0.1 eV Å^{-1}, enough to guarantee fully converged results. In all of the calculations, Brillouin zones were sampled by means of optimal Monkhorst−Pack grids.[12] The generalized gradient approximation Perdew−Burke−Ernzerhof (GGA-PBE) functional was used to account for the exchange-correlation effects,[13] ultrasoft pseudopotentials to model the ion−electron interaction within each atom,[14] and a plane-wave basis set up to a kinetic energy cutoff of 40 and 300 Ry for the charge density. The excitation spectra were obtained as $I(\omega) \propto \omega \mathrm{Im}[\bar{\alpha}(\omega)]$, where $\bar{\alpha}$ is the spherical average (average of the diagonal elements) of the dipole polarizability; an imaginary part of 0.002 Ry was added to the frequency in order to smooth the emerging divergences of the polarizability. Additionally, once the different TDDFT spectra were obtained, we carried out a battery of calculations with the *Gaussian16* package[15] to obtain oscillator strengths and elucidate transitions and electronic states involved in the most intense excitations by using the same GGA-PBE functional and the rather large 6-311G* basis set. To compute the individual transitions, we used the configuration interaction single-excitation (CIS) formalism.[16] This implementation is computationally very demanding but provides excellent results in both closed- and open-shell systems.

Synthesis of the Compounds. *Synthesis of [CuI(TBA)]$_n$ (**1**).* CuI (0.190 g, 1.00 mmol) and TBA (0.137 g, 1.00 mmol) in acetonitrile (MeCN; 10 mL) were mixed and stirred until a homogeneous solution was formed. Then the solvent was removed under vacuum until a red gooey oil was obtained. This oil was sonicated in hexane, resulting in an orange solid after extraction of solvent. This product was washed with diethyl ether and dried under vacuum (0.135 g, 41% yield). Single crystals suitable for X-ray diffraction studies were obtained by heating an equimolar mixture of CuI and TBA at 135 °C for 10 min. Then, the obtained red solid was left to stand in *n*-butyl alcohol overnight, affording orange prismatic crystals of **1**. Elem anal. Calcd for C_7H_7ICuNS: C, 25.66; H, 2.14; N, 4.28; S, 9.79. Found: C, 24.87; H, 2.14; N, 4.16; S, 9.50. FT-IR selected data (KBr, cm^{-1}): 3378 (m), 3225 (m), 3149 (m), 2922 (m), 2854 (m), 1582 (vs), 1441 (m), 1397 (s), 1278 (s), 1168 (s), 1015 (w), 925 (w), 859 (s), 762 (s), 677 (vs).

*Synthesis of {[CuI(TBA)]·THF}$_n$ (**1**·THF) and [CuI(TBA)]·acetone}$_n$ (**1**·acetone).* Single crystals suitable for X-ray diffraction studies were obtained by slow diffusion at RT of *n*-pentane into THF or acetone solutions of **1**. **1**·THF. Elem anal. Calcd for $C_{11}H_{15}ICuNSO$: C, 33.05; H, 3.75; N, 3.50; S, 8.02. Found: C, 32.29; H, 3.63; N, 3.46; S, 8.12. FT-IR selected data (KBr, cm^{-1}): 3242 (m), 3086 (m), 2975 (m), 2871 (m), 1651(s), 1464 (s), 1322 (m), 1303 (s), 1275 (vs), 1183 (m), 1051 (vs), 868 (s), 774 (s), 686 (vs). **1**·acetone. Elem anal. Calcd for $C_{10}H_{13}ICuNSO$: C, 31.14; H, 3.40; N, 3.63; S, 8.31. Found: C, 34.70; H, 3.70; N, 4.15; S, 9.69. FT-IR selected data (KBr, cm^{-1}): 3278 (m), 3148 (s), 1697 (vs), 1642 (vs), 1595 (m), 1463 (m), 1412 (m), 1363 (m), 1310 (m), 1271 (vs), 1225 (vs), 1186 (m), 1088 (m), 870 (vs), 774 (vs), 694 (vs).

*Synthesis of {[CuI(TBA)]·MeOH}$_n$ (**1**·MeOH).* To a solution of CuI (0.190 g, 1.00 mmol) and TBA (0.137 g, 1.00 mmol) in 1 mL of MeCN was added 20 mL of MeOH. This mixture was allowed to stand in a Petri dish at RT. After evaporation of the solvent, orange prismatic crystals, suitable for X-ray diffraction studies, were synthesized. The crystalline product was washed with MeOH and dried at air (0.334 g, 93% yield). Elem anal. Calcd for $C_8H_{11}ICuNSO$: C, 26.71; H, 3.08; N, 3.89; S, 8.91. Found: C, 25.83; H, 2.88; N, 3.72; S, 8.90. FT-IR selected data (KBr, cm^{-1}): 3503 (m), 3253 (m), 3028 (m), 1645 (s), 1449 (s), 1309 (s), 1268 (s), 1141 (m), 1081 (w), 996 (s), 876 (s), 755 (s), 671 (vs).

*Synthesis of [CuI(TBA)$_3$] (**2**).* Following the same procedure as that previously described for **1** but using a 1:5 CuI/TBA ratio [CuI (0.038 g, 0.20 mmol) and TBA (0.137 g, 1.00 mmol)] instead, a yellow solid was isolated after vacuum extraction of the solvent, washed with dichloromethane, and dried under vacuum (0.061 g, 50% yield). Single crystals suitable for X-ray diffraction studies were obtained by *n*-pentane vapor diffusion into a diethyl ether solution of **2**. Elem anal. Calcd for $C_{21}H_{21}ICuN_3S_3$: C, 41.91; H, 3.52; N, 6.98; S, 15.94. Found: C, 42.32; H, 3.59; N, 7.17; S, 15.84. FT-IR selected data (KBr, cm^{-1}): 3344 (m), 3244 (m), 3156 (s), 1606 (vs), 1450 (m), 1318 (m), 1268 (m), 1180 (m), 874 (vs), 770 (vs), 704 (s), 691 (s).

*Synthesis of [Cu$_2$I$_2$(TBA)$_4$]·MeCN (**3**).* An equimolar mixture of CuI (0.762 g, 4.00 mmol) and TBA (0.549 g, 4.00 mmol) in MeCN (2 mL) was sonicated until a homogeneous solution was obtained. Then the solution was left to stand overnight, whereupon **3** precipitated as orange prismatic crystals, suitable for X-ray diffraction analysis. The crystalline product was filtered off, washed with a water/MeCN (1:1) solvent mixture, and dried in air (0.146 g, 14% yield). Elem anal. Calcd for $C_{30}H_{31}I_2Cu_2N_5S_4$: C, 37.12; H, 3.22; N, 7.21; S, 13.21. Found: C, 36.53; H, 3.16; N, 7.18; S, 13.03. FT-IR selected data (KBr, cm^{-1}): 3334 (m), 3247 (m), 3157 (m), 2252 (w), 1611 (vs),

DOI: 10.1021/acs.inorgchem.8b03364
Inorg. Chem. XXXX, XXX, XXX−XXX

1442 (m), 1418 (m), 1311 (m), 1265 (s), 1211 (s), 1170 (m), 1028 (w), 926 (w), 877 (s), 768 (m), 687 (vs).

Synthesis of $[Cu_3I_3(TBA)_2]_n$ *(4).* Compound **4** was prepared following a slight modification of the process used for **1**·MeOH. Thus, to a solution of CuI (0.190 g, 1.00 mmol) and TBA (0.137 g, 1.00 mmol) in MeCN (1 mL) was added 20 mL of MeOH. Then, the mixture was stirred for 1 h, and the resulting yellow solid was washed with MeOH and diethyl ether and dried under vacuum (0.134 g, 48% yield). Single crystals for X-ray diffraction analysis were obtained by *n*-pentane vapor diffusion into an equimolar solution of CuI and TBA in 2:1 MeOH/MeCN. Elem anal. Calcd for $C_{14}H_{14}I_3Cu_3N_2S_2$: C, 19.88; H, 1.67; N, 3.31; S, 7.58. Found: C, 19.93; H, 1.84; N, 3.28; S, 7.56. FT-IR selected data (KBr, cm^{-1}): 3346 (m), 3245 (m), 3159 (m), 1601 (vs), 1441 (m), 1420 (m), 1316 (s), 1258 (s), 1211 (s), 1150 (s), 1027 (w), 925 (w), 866 (s), 763 (s), 685 (vs).

Synthesis of $[CuBr(TBA)]_n$ *(5).* An equimolar solution of CuBr (0.143 g, 1.0 mmol) and TBA (0.137 g, 1.00 mmol) in MeCN (20 mL) was stirred at RT for 30 min. After solvent removal in a vacuum, the obtained orange solid was washed with diethyl ether and dried under vacuum (0,171 g, 61% yield). Orange prismatic single crystals, suitable for X-ray diffraction studies, were obtained by slow evaporation of a solution of **5** in MeCN at RT. Elem anal. Calcd for $C_7H_7BrCuNS$: C, 29.97; H, 2.51; N, 4.99; S, 11.40. Found: C, 30.34; H, 2.62; N, 5.16; S, 11.18. FT-IR selected data (KBr, cm^{-1}): 3267 (m), 3082 (m), 1628 (s), 1456 (s), 1306 (m), 1258 (s), 1184 (m), 1128 (w), 1073 (w), 926 (w), 850 (s), 765 (s), 679 (vs).

Synthesis of $\{[CuBr(TBA)]\cdot THF\}_n$ *(5·THF) and* $[CuBr(TBA)]\cdot acetone\}_n$ *(5·acetone).* By a procedure similar to that previously described for **1**·THF and **1**·acetone, by slow *n*-pentane diffusion into THF or acetone solutions of **5**, suitable crystals for X-ray diffraction of **5**·THF and **5**·acetone were obtained. **5**·THF. Elem anal. Calcd for $C_{11}H_{15}BrCuNSO$: C, 37.46; H, 4.29; N, 3.97; S, 9.07. Found: C, 37.40; H, 4.24; N, 3.89; S, 8.96. FT-IR selected data (KBr, cm^{-1}): 3254 (m), 3090 (m), 2952 (m), 2865 (m), 1652 (s), 1595 (m), 1459 (s), 1304 (vs), 1276 (vs), 1183 (m), 1048 (vs), 865 (s), 775 (s), 688 (vs). **5**·acetone. Elem anal. Calcd for $C_{10}H_{13}BrCuNOS$: C, 35.46; H, 3.87; N, 4.14; S, 9.47. Found: C, 34.71; H, 3.70; N, 4.14; S, 9.69. FT-IR selected data (KBr, cm^{-1}): 3233 (m), 3073 (m), 1696 (vs), 1658 (m), 1456 (m), 1420 (m), 1364 (m), 1324 (m), 1305 (s), 1280 (s), 1231 (s), 883 (m), 767 (vs), 691 (vs).

Synthesis of $\{[CuI(DTBA)]\cdot DMF\}_n$ *(6·DMF).* A solution of DTBA (0.098 g, 0.50 mmol) in DMF (1 mL) was added to a solution of CuI (0.095 g, 0.50 mmol) in MeCN (20 mL), and the mixture was stirred at RT for 1 h. The orange solid obtained was washed with MeCN/DMF (10:1) and diethyl ether and dried under vacuum (0.210 g, 91% yield). Single crystals suitable for X-ray diffraction studies were obtained by diffusion of an MeCN solution of CuI into a solution of DTBA in DMF at RT. Elem anal. Calcd for $C_{11}H_{15}ICuON_3S_2$: C, 28.73; H, 3.29; N, 9.14; S, 13.95. Found: C, 28.78; H, 3.32; N, 9.29; S, 13.85. FT-IR selected data (KBr, cm^{-1}): 3421 (s), 3259 (s), 3157 (m), 2916 (m), 1610 (s), 1435 (m), 1319 (m), 1265 (m), 1014 (w), 877 (w), 847 (w).

Synthesis of $\{[CuI(DTBA)]\cdot 2MeCN\}_n$ *(6·2MeCN) and* $\{[CuI(DTBA)]\cdot MeCN\}_n$ *(6·MeCN).* A mixture of DTBA (0.019 g, 0.10 mmol) and CuI (0.019 g, 0.10 mmol) in MeCN (250 mL) was refluxed for 30 min. An orange solution was obtained, which was filtered off and left at RT, giving rise to orange crystals of **6**·2MeCN suitable for structure determination by X-ray diffraction. When these crystals were separated by filtration, washed with MeCN and diethyl ether, and dried under vacuum, **6**·MeCN was obtained (0.028 g, 65% yield). **6**·MeCN. Elem anal. Calcd for $C_{10}H_{11}ICuN_3S_2$: C, 28.08; H, 2.59; N, 9.82; S, 14.99. Found: C, 28.17; H, 2.67; N, 9.63; S, 14.90. FT-IR selected data (KBr, cm^{-1}): 3344 (m), 3253 (m), 3172 (m), 2281 (w), 2250 (w), 1628 (m), 1608 (s), 1434 (s), 1315 (m), 1263 (m), 1012 (w), 877 (m), 845 (m), 642 (m).

The phase purity of the as-synthesized compounds was confirmed by PXRD (Figures S24–S34).

RESULTS AND DISCUSSION

Synthesis and Structure of TBA-Based Compounds. The synthetic route to this new class of CuX/TBA (X = I, Br)-based compounds is given in Scheme 1. By mixing equimolar amounts of CuI and TBA ligand in MeCN at RT, no precipitation from the solution was observed, but after solvent removal, a red oil was obtained, leading after treatment with *n*-hexane to polycrystalline **1**. Interestingly, despite its polymeric structure, **1** could be dissolved in THF and acetone, affording the corresponding solvated 1D CPs **1**·THF and **1**·acetone, respectively, after vapor diffusion of *n*-pentane. Analogous compound **1**·MeOH was synthesized by a direct reaction between CuI and TBA in a MeOH/MeCN (10:1) solvent mixture.

Scheme 1. Synthetic Routes of CuX/TBA (X = I, Br) Coordination Compounds Formation

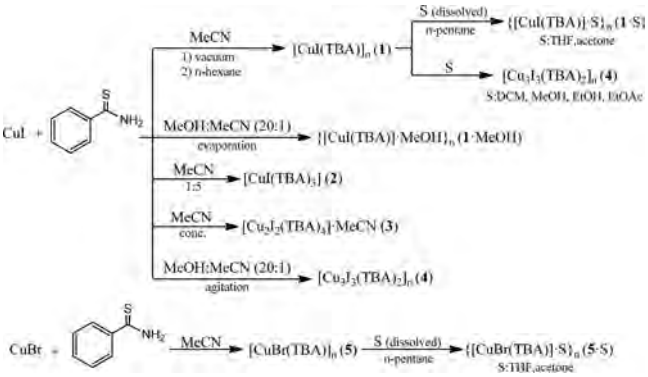

Compounds **1** and **1**·S (S = THF, acetone, MeOH) display 1D polymeric chains, as depicted in Figure 1, parallel to the shortest cell axis (*b* in **1** and *a* in the solvated crystals). In all of these cases, the asymmetric unit contains one ligand, one iodine atom, and one copper(I) atom, plus one solvent molecule in the case of the structures **1**·THF, **1**·acetone, and **1**·MeOH (Figures S1–S4).

Within the 1D chains, the copper atom is coordinated to two TBA ligands via the sulfur atom and to two iodine atoms in a CuI_2S_2 environment. Additionally, Cu–Cu interactions can also be present, and the Cu–Cu distances are influenced by the presence of interstitial solvent molecules (Tables S39–S46). The polymeric chains contain alternating Cu_2I_2 and Cu_2S_2 rhombi at nearly perpendicular angles (80.98, 83.36, 82.33, and 81.73° for **1**, **1**·THF, **1**·acetone, and **1**·MeOH, respectively).

Regarding the supramolecular arrangements, in compound **1**, there are weak interchain N–H···I interactions, while stronger intrachain N–H···I hydrogen-bonding interactions are present (Table S63). In the solvated cocrystals, there are also intrachain hydrogen bonds; additionally, the interstitial solvent molecules in these structures are joined to the chains by N–H···O hydrogen bonds in all of the cases (Table S63 and Figure S15). There are also weaker supramolecular O–H···S and O–H···I bonds in **1**·MeOH (Table S63).

The crystals of **1** and **1**·S adopt a needle or ribbon-like habit, and it was determined by indexation of the crystal faces that the CP chains in these crystals are, in all of these cases, oriented parallel to the length of the crystals (Figures S20 and S21).

DOI: 10.1021/acs.inorgchem.8b03364
Inorg. Chem. XXXX, XXX, XXX–XXX

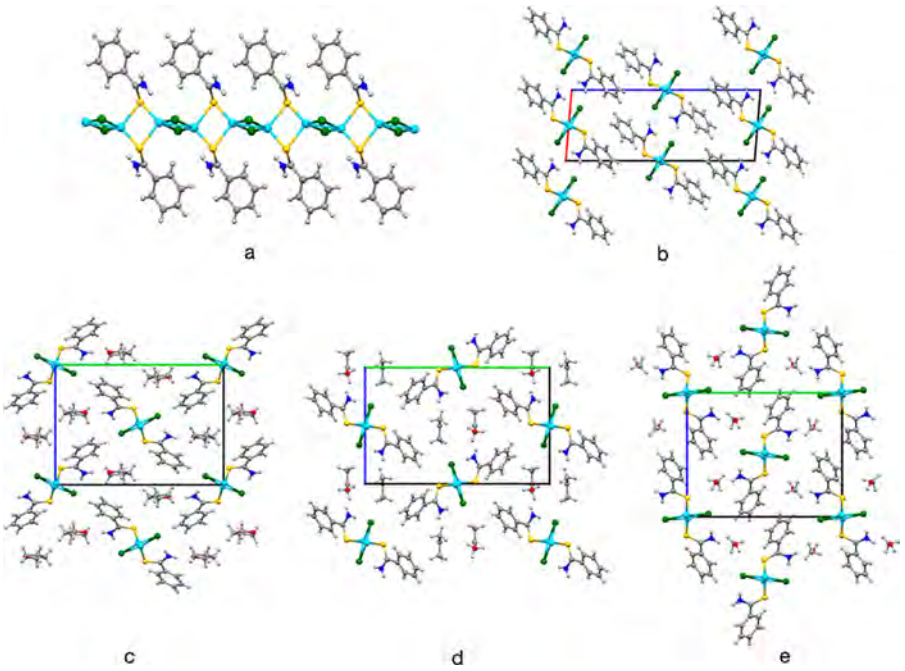

Figure 1. Lateral view of the 1D CP of **1** (a) and packing of the chains in the structures of **1** (b), **1**·THF (c), **1**·acetone (d), and **1**·MeOH (e). Color code: Cu, cyan; I, green; S, yellow; N, dark blue; O, red; C, gray; H, white.

We also analyzed the influence of the stoichiometric ratio and concentration of the reagents in the process of preparation. Thus, solutions with 2:1 and 1:2 CuI/TBA ratios in MeCN were treated in the same manner, but **1** was obtained in all of these cases. Only when a large excess of TBA was used (5 equiv), the molecular compound **2** was isolated showing a $[CuI(TBA)_3]$ molecule per asymmetric unit (Figures 2a and S5). The copper(I) atom in this compound shows a tetrahedral $CuIS_3$ environment, where the TBA ligands are coordinated by the sulfur atom. There are N−H···I interactions (both intra- and intermolecular) and N−H···S hydrogen bonds between the $[CuI(TBA)_3]$ molecules. Compound **2** was found to be isostructural with the previously reported chlorine derivative $[CuCl(TBA)_3]$.[17]

In addition, when equimolar MeCN solutions of CuI and TBA at high concentrations (≥1 M) were left to stand undisturbed, the dimeric molecular complex **3**, Figure 2b was obtained as a crystalline product. The asymmetric unit of **3** contains one copper(I) atom, one iodine atom, two TBA ligands, and one MeCN interstitial molecule (Figure S6). This complex could be described as a molecular precursor of the **1** CP chains, also showing the CuS_2I_2 coordination environment and the Cu_2I_2 rhombus observed in **1** and **1**·S. The packing of the dimers in the crystal could be described as chains of dimers joined by N−H···S bonds along the *b* axis, with the solvent molecules bonded to the dimers by N−H···N hydrogen bonds (Figure S16), analogous to the N−H···O bonds observed in the solvated cocrystals of **1**. This dimeric molecule is similar to the previously reported $[Cu_2I_2(TAA)_4]$.[9b] Interestingly, the Cu−Cu distance in $[Cu_2I_2(TBA)_4]$ was found to be considerably shorter (3.379 Å at 296 K) than the one in $[Cu_2I_2(TAA)_4]$, 3.678 Å for the structure solved with the data set collected at the same temperature. This distance gets shortened, as expected, in the structure of $[Cu_2I_2(TBA)_4]$ solved from the data collected at low temperature (3.320 Å).

During our investigations, the transformation of **1** into 1D CP **4** was observed after immersion of **1** in several solvents

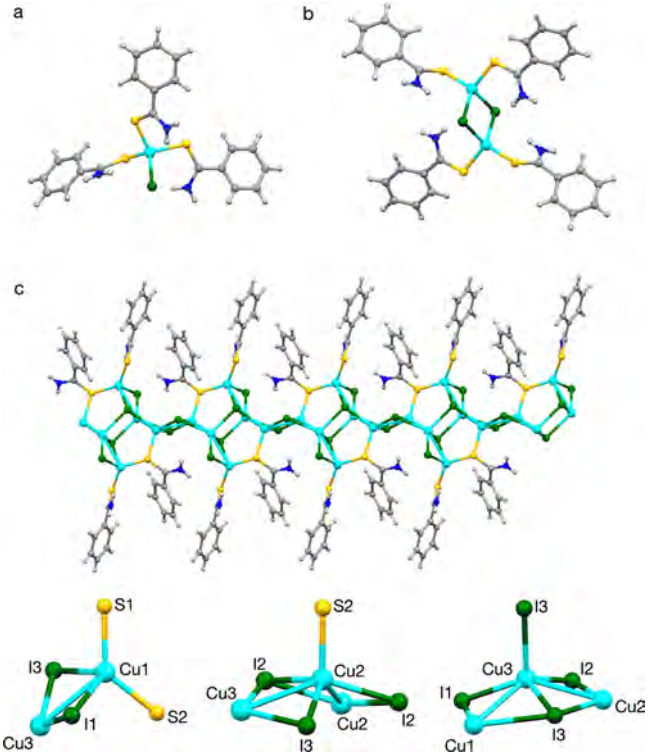

Figure 2. Molecular coordination compounds **2** (a) and **3** (b). The solvent molecules in **3** have been omitted. (c) Polymeric $[Cu_3I_3(TBA)_2]_n$ chain found in **4** (top) and copper environments for the three crystallographically independent copper atoms (bottom). Color code: Cu, cyan; I, green; S, yellow; N, dark blue; O, red; C, gray; H, white.

(Figure S34). The direct synthesis of **4** was carried out by stirring a equimolar solution of CuI and TBA in a MeOH/MeCN (20:1) solvent mixture, as shown in Scheme 1. Compound **4** displays a 1D structure that is different from

DOI: 10.1021/acs.inorgchem.8b03364
Inorg. Chem. XXXX, XXX, XXX−XXX

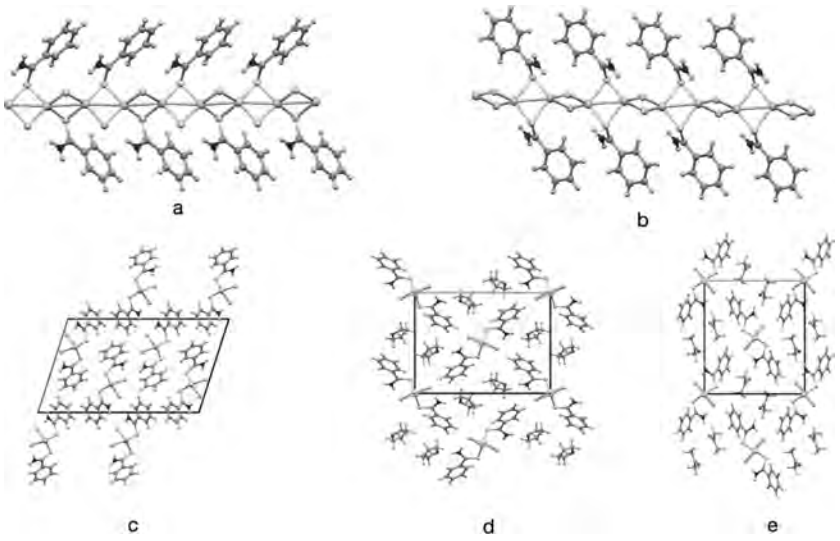

Figure 3. Lateral view of the 1D CP of **5** (a) and **5**·S (b) where S = THF or acetone. Packing of the chains in the structures of **5** (c), **5**·THF (d), and **5**·acetone (e). Color code: Cu, cyan; I, green; S, yellow; N, dark blue; O, red; C, gray; H, white.

that observed in compound **1**, as well as a different stoichiometry. The asymmetric unit contains three copper(I) centers, three iodine atoms, and two TBA ligands (Figure S7). One of the TBA ligands shows the same coordination mode as that observed in compound **1** (sulfur-donor monotopic), but the other ligand is acting as a μ_2-sulfur between copper atoms Cu1 and Cu2 (Figure 2c). Regarding the iodine atoms, μ_2-I1 binds the metal centers Cu1 and Cu3, while μ_3-I2 connects to three copper atoms (Cu2, Cu2, and Cu3) and μ_4-I3 joins four metal centers (Cu1, Cu2, and Cu3). The three copper atoms in the asymmetric unit also display different environments, involving metal−metal interactions added to the tetrahedral environment (Figure 2c, bottom). Unfortunately, these metal−metal interactions do not propagate along the full length of the CP, yielding only six-membered chains (Cu1−Cu3−Cu2−Cu2−Cu3−Cu1), as depicted in Figure S8.

The chains are packed in the crystal by van der Waals forces, while intrachain strong N−H···S and weaker N−H···I interactions can be observed. The orientation of the chains in the needle-shaped crystals was studied by indexation of the faces in the measured crystals, and it was observed that the polymeric chains were oriented parallel to the longest axis of the single crystals (Figure S22).

For comparison, we also carried out the direct reaction between CuBr and TBA in MeCN at RT, giving rise to the formation of **5**. This 1D polymeric compound displays the same formula as the iodine derivative **1**, although there are important structural differences between the two CPs (Figure 3a). The asymmetric unit in **5** (Figure S9) is twice that found in **1** (containing two copper atoms, two TBA ligands, and two bromine atoms). More significantly, in the chains observed in compound **1** as well as in the solvated cocrystals, there are alternating Cu_2I_2 and Cu_2S_2 rhombi, while in the chains present in **5**, there is only a Cu_2IS rhombus (with an angle between consecutive rhombi of 83.86). This leads to very similar Cu−Cu distances in **5**, while in **1** and the solvated compounds, there are alternating shorter and longer ones. The different supramolecular arrangement of the chains in **5** compared to that observed in **1** is remarkable. In the bromine derivative, N−H···Br interactions involving atoms within the same chain and from neighboring ones are very similar, while in compound **1**, the interactions between atoms from adjacent 1D polymers are considerably weaker.

Similarly to **1**, solubilization of **5** in THF and acetone allowed us to synthesize the corresponding **5**·THF and **5**·acetone, respectively. These compounds show a 1D CP analogous to the iodine derivatives, with the same alternating Cu_2I_2 and Cu_2S_2 rhombi pattern (Figure 3e). The asymmetric unit in both cocrystals of **5** is analogous to the corresponding solvated compounds of **1**, as shown in Figures S10 and S11, and their supramolecular arrangement is also very similar (Figures 3 and S17); in particular, **1**·THF and **5**·THF were found to be fully isostructural. In the case of **5**, no transformations were noticed, as shown in Figure S36.

The crystals of compound **5** also adopt a needle or ribbon-like habit, and it was determined by indexation of the crystal faces that the CP chains in the solid state of **5** are, as happened with compound **1**, oriented parallel to length of the crystals (Figure S23).

Synthesis and Structure of DTBA-Based Compounds. We further explored the assembly of the ditopic ligand DTBA with CuI. Thus, the equimolar reaction between CuI and DTBA in a MeCN/DMF (20:1) solvent mixture at RT led to the 2D CP $\{[CuI(DTBA)]\cdot DMF\}_n$ (**6**·DMF). The synthesis of CuI/DTBA-based compounds is gathered in Scheme 2. When **6**·DMF was soaked in MeCN or MeOH, the exchange of guest solvent molecules took place and **6**·S (S = MeCN, MeOH) was obtained. The exchange of the solvent molecules was confirmed by FT-IR analysis (Figure S37). Besides, **6**·S

Scheme 2. Synthetic Routes of CuI/DTBA Coordination Compounds Formation

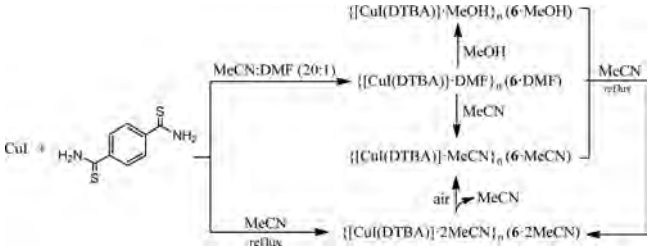

DOI: 10.1021/acs.inorgchem.8b03364
Inorg. Chem. XXXX, XXX, XXX−XXX

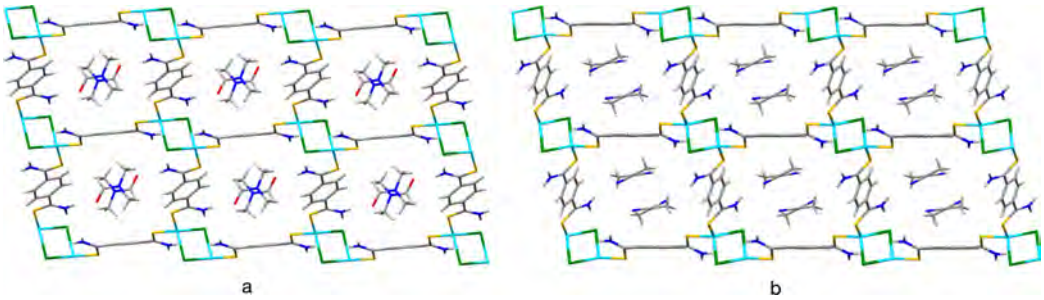

Figure 4. View of the 2D CPs parallel to the (011) plane in **6**·DMF (a) and **6**·2MeCN (b). Color code: Cu, cyan; I, green; S, yellow; N, dark blue; O, red; C, gray; H, white.

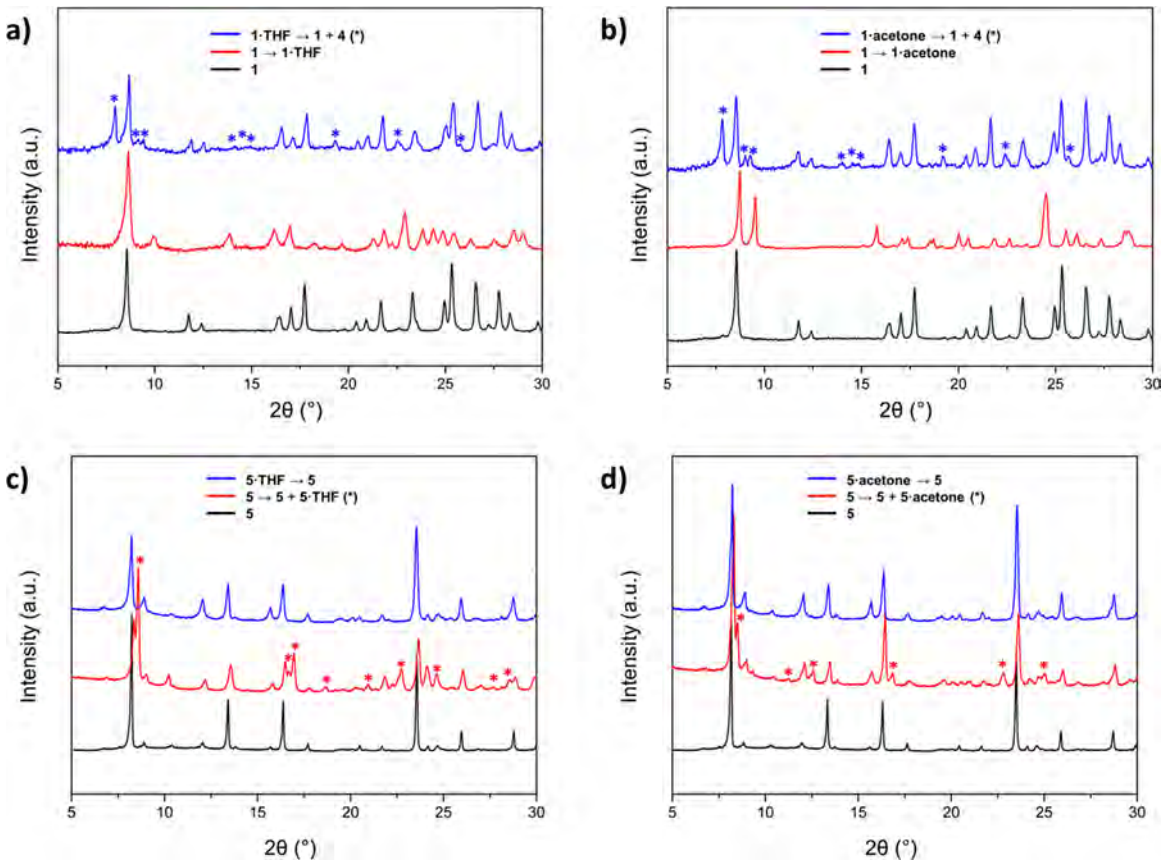

Figure 5. PXRD patterns of **1** (a and b) and **5** (c and d) before (black) and after exposure to THF or acetone vapors for 24 h at RT (red) and subsequent heating at 80 °C under vacuum for 12 h (blue). The asterisks indicate the peaks corresponding to the **4** (a and b), **5**·THF (c), and **5**·acetone (d) phases.

compounds displayed similar PXRD patterns (Figure S38), confirming similar structures.

Otherwise, the reaction between CuI and DTBA (1:1) in refluxing MeCN allowed one to obtain single crystals of **6**·2MeCN. However, crystals of **6**·2MeCN easily undergo a partial solvent loss under ambient conditions, giving rise to **6**·MeCN (Figure S39). Furthermore, **6**·2MeCN crystals could also be obtained from hot MeCN solutions of **6**·S (S = DMF, MeCN, MeOH).

Compounds **6**·DMF and **6**·2MeCN both display a 2D polymeric structure where the layers are parallel to the *bc* plane, with the solvent molecules lodged in the square interstitial spaces (Figure 4). In both cases, the asymmetric unit entails a copper(I) atom, an iodine atom, and the halves of the DTBA ligand, plus one DMF solvent molecule (**6**·DMF) or two MeCN ones (**6**·2MeCN), as depicted in Figures S12 and S14. The copper atom displays a CuI_2S_2 coordination environment, while the DTBA ligands are coordinated to one metal atom by each of the two opposite sulfur atoms and the iodine atom is bridging two copper(I) atoms, yielding Cu_2I_2 rhombi.

The solvent molecules are joined to the 2D polymeric layers by N−H···O bonds in **6**·DMF (Figure S18). In the structure of **6**·2MeCN, it is interesting to note that the two solvent molecules are not equally bonded to the 2D framework: one of the MeCN molecules is joined to the CP layer by a N−H···N bond (Figure S19), while the second one is only weakly bonded to the former one by a C−H···N interaction (Table S67). This fact could explain the easy loss of one of the solvent molecules in **6**·2MeCN to yield **6**·MeCN. It was also observed that **6**·2MeCN was not stable in normal conditions, and for

DOI: 10.1021/acs.inorgchem.8b03364
Inorg. Chem. XXXX, XXX, XXX−XXX

this compound, only X-ray diffraction data at low temperature could be collected to solve the crystal structure.

Thermal Stability. Thermogravimetric analysis (TGA) of all synthesized CuX/TBA (X = I, Br) 1D CPs **1**, **1**·S (S = THF, acetone, MeOH), **4**, **5**, and **5**·S (S = THF, acetone) was carried out under a nitrogen atmosphere (Figures S40−S47 and Table S68). For solvated compounds (**1**·S and **5**·S), upon heating, an initial solvent loss process was observed, with well-defined plateaus above ca. 100 °C. At higher temperatures, all compounds show a weight loss step between 250 and 275 °C, which could be assigned to the loss of a TBA ligand.

The thermal stability of **6**·S (S = DMF, MeCN, MeOH) was also evaluated. Results showed an analogous thermal behavior for all of the compounds (Figures S48−S50 and Table S69). Thus, TGA curves displayed an initial weight loss, which corresponded to the loss of one solvent molecule. Then, decomposition of the frameworks occurred in two consecutive steps, which corresponded to the loss of half of the DTBA molecules. Additionally, the thermal stability of **6**·DMF was examined by PXRD after the samples were heated at different temperatures for 1 h (Figure S51). Hence, when **6**·DMF was heated above ca. 100 °C, a new phase was found. FT-IR and elemental analysis characterization of the solid heated at 225 °C (Figure S52 and Table S70) revealed a chemical composition of Cu_2I_2(DTBA), which corresponds to the loss of half of the DTBA ligand observed in TGA.

Vapor-Assisted Structural Transformations. The obtention of solvated and desolvated 1D networks prompted us to study the solvation/desolvation processes displayed by these compounds. To this end, experiments were followed up (ex situ) by PXRD to assess any phase changes. Initially, **1** and **5** were exposed to THF, acetone, and MeOH vapors for 24 h at RT in attempts to facilitate the inclusion of solvent guest molecules. Interestingly, after **1** exposure to THF and acetone vapors, the corresponding solvated CPs **1**·THF and **1**·acetone were formed, respectively (Figure 5a,b). The resulting solids were placed under vacuum for 24 h at RT, but no changes were detected. Then, solvated **1**·THF and **1**·acetone were heated at 80 °C under vacuum for 12 h, showing that solvent loss (**1**·S → **1**) was accompanied by concomitant formation of **4**. In the case of **5**, after exposure to THF and acetone vapors, both solvated and desolvated species (**5** + **5**·S) were identified (Figure 5c,d), indicating that transformation was not fully achieved. This can be attributed to the required rearrangement of the Cu_2IS rhombi in **5** to form alternating Cu_2I_2 and Cu_2S_2 rhombi to give rise to solvated species **5**·S. Then, the solvent removal was performed under the same conditions (80 °C in a vacuum, 24 h), yielding desolvated compound **5**. Otherwise, no phase changes were detected after **1** and **5** exposure to MeOH vapor.

Luminescent Properties. Much research interest has recently focused on the luminescent properties of CPs because of their potential applications as light-emitting diodes.[18] Indeed, some copper(I) complexes have shown rich structural variety combined with bright luminescence, even at RT, and emissive behavior that can be modulated with the structure and environment.[19] This fact prompted us to investigate the luminescent properties of the synthesized compounds in the solid state upon excitation with a UV lamp (λ_{exc}= 365 nm). At RT, **1**, **1**·acetone, and **1**·MeOH showed by the naked eye orange emission, while no emission was observed for the other compounds. Moreover, when crystalline samples of **1**, **1**·S (S = THF, acetone, MeOH), **5**, and **5**·S (S = THF, acetone) were immersed in liquid nitrogen and exposed to irradiation of the same UV lamp, a clearly orange emission was observed. These changes were distinguished by the naked eye and recorded by a digital camera (Figure 6). These processes are fully reversible

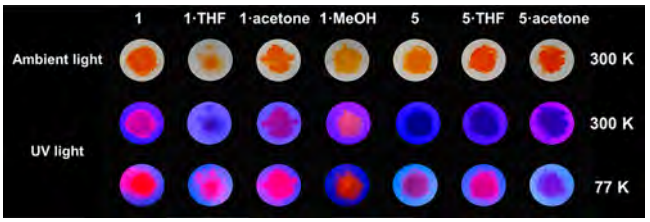

Figure 6. Photographs of solid samples of 1D CPs **1**, **1**·S (S = THF, acetone, MeOH), **5**, and **5**·S (S = THF, acetone) under ambient light and UV-lamp irradiation at 356 nm at RT (300 K) and in liquid nitrogen (77 K).

for all compounds returning to their initial state after they were allowed to stay at RT for a few seconds. However, when compounds **2**−**4** and **6**·S (S = DMF, MeCN, MeOH) were immersed in liquid nitrogen and then exposed to UV irradiation, using the same UV lamp, no change was observed (Figure S53).

In order to check for the possible presence of emission arising from the ligand, free TBA ligand was investigated. Solid-state emission spectra at RT (λ_{exc}= 359 nm) showed very weak emission in the high-energy region with maxima centered at ca. 424, 471, 483, and 493 nm, being assigned to ligand-centered $\pi \rightarrow \pi^*$ transitions (Figure S54). These bands appeared to be very weak in the blue region for **1**, **1**·S, **5**, and **5**·S CPs.

To gain more insight into the nature of the modest but fully reversible thermochromic effects found for all **1**, **1**·S (S = THF, acetone, MeOH), **5**, and **5**·S (S = THF, acetone) compounds, the emission spectra were registered at variable temperature (from 300 to 100 K, λ_{exc}= 450 nm). For **1** and **1**·S (S = THF, acetone, MeOH), at RT, weak broad bands with maxima centered at ca. 635, 630, 630, and 611 nm were observed. When the temperature was lowered, broad and unstructured bands began to appear, increasing their intensity as the temperature was decreased. For **1** and **1**·MeOH, this broad band was progressively resolved as the temperature was decreased, showing maxima centered at ca. 630 and 607 nm, respectively, at 80 K. **1**·THF and **1**·acetone showed similar behavior: a broad band centered at 630 nm was observed at 240 K, and as the temperature was decreased, narrowing down from 100 K, bands centered at 615 and 626 nm, respectively, were observed, together with a shoulder to lower energy (670 nm for **1**·THF) and another band at 657 nm for **1**·acetone (Figure 7). The emission lifetimes at 100 K were in the range of 11 μs (**1**) to 16 μs (**1**·S), and this microsecond time scale was indicative of an emission arising from a triplet state.

The isostructural CPs based on copper bromide, **5** and **5**·S (S = THF, acetone), showed lower emission than the analogous copper iodide CPs **1** and **1**·S. From RT up to 180 K, they were not luminescent. However, when the temperature was decreased, weak broad emission bands began to appear, and at 80 K, broad bands centered at ca. 620, 682, and 638 nm were observed (Figure 8). The emission lifetimes at 100 K were close to 10 μs, being also indicative of an emission arising from a triplet state.

DOI: 10.1021/acs.inorgchem.8b03364
Inorg. Chem. XXXX, XXX, XXX−XXX

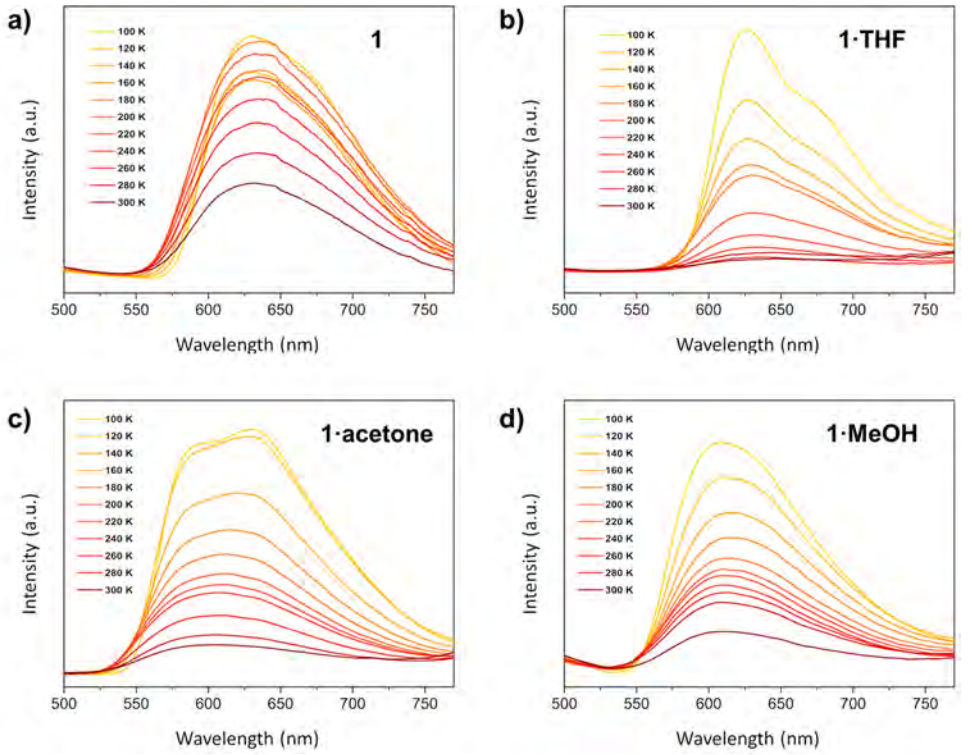

Figure 7. Temperature-dependent luminescence spectra of **1**·S (S = THF, acetone, MeOH) from 300 K down to 100 K in the solid state (λ_{exc}= 450 nm; ΔT = 20 K).

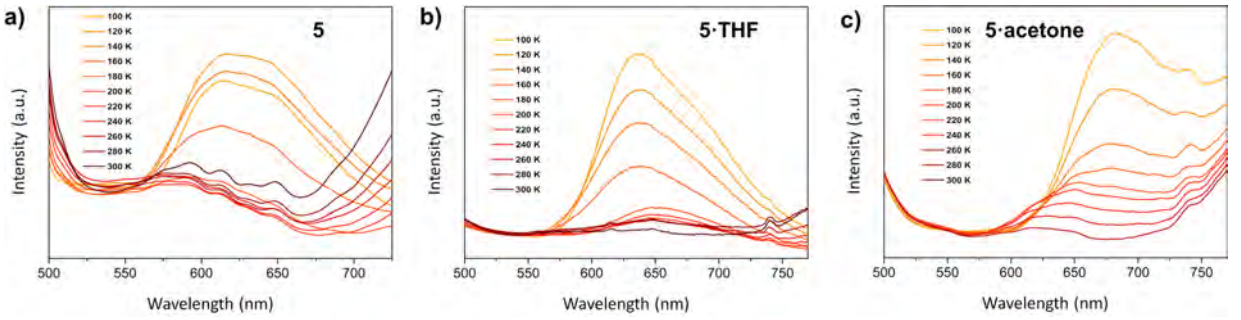

Figure 8. Temperature-dependent luminescence spectra of **5** and **5**·S (S = THF, acetone) from 300 K down to 100 K in the solid state (λ_{exc}= 450 nm; ΔT = 20 K).

According to previous studies related to CPs based on copper halide, the origin of the observed emission centered around 610−680 nm might be derived from an excited-state halide-to-ligand charge transfer (^{3}XLCT) in character, which is itself a combination of ^{3}XLCT and metal-centered transfer (^{3}MCC; $3d^{10} \rightarrow Cu\ 3d^9 4s^1$), with this ^{3}MCC contribution being very sensible to Cu···Cu distances.[3a,20] The nature of the emission spectra, with broad and unstructured bands, is also in agreement with the assignation made as a combination of ^{3}(M+X)LCT states.[21]

In order to deeply understand the nature of the origin of the observed thermochromism, the crystal structures for **1**, **1**·S (S = THF, acetone, MeOH), **5**, and **5**·S (S = THF, acetone) were determined by single-crystal X-ray diffraction analysis at 110 K. As shown in Table 1, in all compounds, a slight decrease of the cell parameters is observed; together with that, at lower temperature, for isostructural **1**, **1**·S (S = THF, acetone, MeOH) **5** and **5**·S (S = THF, acetone) compounds, a shortening of Cu···Cu interactions is observed as Δ = 0.09 and 0.056 nm for **1**, Δ = 0.07 and 0.045 nm for **1**·acetone, Δ = 0.023 and 0.060 nm for **1**·THF, and Δ = 0.022 and 0.047 nm for **1**·MeOH for Cu_2I_2 and Cu_2S_2 rhomboids and Δ = 0.025 and 0.025 nm for **5**, Δ = 0.009 and 0.00 nm for **5**·acetone, and Δ = 0.023 and 0.060 nm for **5**·THF for Cu_2Br_2 and Cu_2S_2 rhomboids. These shortenings in the unit cell parameter and in the Cu···Cu distances at lower temperature are in accordance with the assignments made as a combination of ^{3}(M+X)LCT states,[21] where the contribution of the ^{3}MCC transition to the emission is stronger when the Cu···Cu distances are shorter. Comparing the Cu···Cu distances for Cu_2X_2 rhomboids, we can observe that compounds containing Cu_2I_2 units (**1** and **1**·S) show shorter values (between 2.680 and 2.941 Å) than the analogues with Cu_2Br_2 units (**5** and **5**·S; 2.857−3.001 Å). These facts are in agreement with the higher emission observed for compounds based on copper iodide (**1** and **1**·S) with respect to those containing copper bromide (**5** and **5**·S) and support the ^{3}MCC contribution in the emission. This is also supported by the DFT calculations carried out, where the

DOI: 10.1021/acs.inorgchem.8b03364
Inorg. Chem. XXXX, XXX, XXX−XXX

Table 1. Selected Bond Lengths for Compounds 1, 1·S (S = THF, Acetone, MeOH), 5, and 5·S (S = THF, Acetone) at Different Temperatures

	temp (K)	Cu−Cu (Å)	Cu−X (Å)	Cu−S (Å)
1	296	2.689(2)	2.612(1)	2.277(2)
		2.967(2)	2.650(1)	2.511(2)
	110	2.940(3)	2.622(2)	2.295(2)
		3.003(3)	2.629(2)	2.534(3)
1·THF	296	2.940(3)	2.622(2)	2.295(2)
		3.003(3)	2.629(2)	2.534(3)
	110	2.917(2)	2.627(1)	2.295(1)
		2.969(2)	2.638(1)	2.480(1)
1·acetone	296	2.869(2)	2.6137(8)	2.292(2)
		2.876(1)	2.6356(8)	2.529(2)
	110	2.815(1)	2.6149(7)	2.295(1)
		2.870(1)	2.6319(7)	2.480(1)
1·MeOH	296	2.7128(9)	2.6118(5)	2.294(1)
		2.743(1)	2.6583(5)	2.503(1)
	110	2.6914(6)	2.6158(3)	2.2963(7)
		2.6963(6)	2.6526(3)	2.4726(7)
5	250	2.857 (3)	2.498(3)	2.280 (5)
		2.885 (3)	2.600 (3)	2.341 (5)
		2.885 (3)	2.600 (3)	2.342 (5)
			2.581(3)	2.271 (5)
			2.494(3)	
	110	2.832(4)	2.498(3)	2.274(5)
		2.860(4)	2.595(3)	2.341(5)
		2.860(4)	2.595(3)	2.336(5)
			2.575(3)	2.265(5)
			2.496(3)	
5·THF	296	2.824 (1)	2.4674 (8)	2.498 (2)
		3.001 (1)	2.4931 (8)	2.274 (1)
	110	2.7640 (9)	2.4749 (6)	2.445 (1)
		2.9781 (9)	2.4738 (6)	2.271 (1)
5·acetone	200	2.813 (3)	2.475 (2)	2.270 (3)
		2.989 (2)		2.471 (3)

valence band (VB) is mostly formed by electronic states from the metallic chain, while the conduction band (CB) and its closest empty states are formed by electronic states located on the organic ligands, thus allowing tunability of the compounds. In addition, the increase observed in the emission intensity upon cooling is due to an increase in the structural rigidity, decreasing the nonradiative rate constant.

The photoluminescent spectra for **1**·S (S = acetone, THF, MeOH) are slightly dependent on the solvent molecules, with **1**·THF showing higher emission. This observation could be attributed to a stronger hydrogen bond, with a N−H···O distance (1.98 Å) shorter than those in **1**·acetone (2.04 Å) and **1**·MeOH (2.06 Å).

Finally, the ^{3}(M+X)LCT band for **1**−**4** compounds is assigned based on the fact that related CPs containing thioacetamide ligands $[CuX(TAA)]_n$ (X = Br, I) instead of TBA ligands are nonemissive in this region.[9a] This feature could be attributed to the lack of π^* orbitals necessary for the ^{3}XLCT process.

Therefore, we can conclude that, for **1**−**4** compounds, the emission bands, observed at RT, are due to a combination of ^{3}XLCT and ^{3}MCC states, while at lower temperatures, a higher contribution of ^{3}MCC (Cu d^{10} → Cu d^9s^1) bands takes place. These studies show direct evidence suggesting that thermochromic luminescence of these compounds is caused by temperature dependence, which affect the Cu···Cu distances, with these Cu···Cu interactions being the key parameter determining the ^{3}CC transitions affecting their luminescence.

Electrical Conductivity. The electrical conductivity of the obtained CPs was evaluated in the solid state at 25 °C by using the two-contact method with a graphite paste contact (Figure S55). The conductivity values obtained under these conditions are summarized in Table 2.

Table 2. Electrical Conductivity Values Obtained for the Different CPs at 25 °C Using a Two-Contact Method and Average Cu−Cu, Cu−X, and Cu−S Distances

	conductivity (S cm^{-1})	CB−VB gap (eV)
1[a]	3.3×10^{-11}	1.38
1·acetone[b]	1.3×10^{-8}	1.22
1·MeOH[b]	1.15×10^{-9}	1.36
4[b]	1.7×10^{-10}	1.29
5[a]	3.6×10^{-8}	1.23
5·THF[b]	1.9×10^{-7}	1.21
5·acetone[b]	1.5×10^{-9}	1.27

[a]Pellet. [b]Crystal.

The data obtained show that these CPs have a relatively low conductivity, within the range of semiconductor materials, with no significant differences between them. The electrical conductivity of closely related 1D CPs based on $Cu_2I_2S_2$ chains, similar to that shown in compound **1**, has recently been reported, showing semiconductor behavior and a conductivity value of 6.8×10^{-9} S cm^{-1} at 25 °C.[22] This is quite in agreement with the values obtained for compounds **1** and **1**·S (S = THF, acetone, MeOH). Others related 2D and 3D CPs with both sulfur and iodine atoms acting as bridging ligands, and similar Cu−S−Cu−I chains show conductivity values in the range 10^{-7}−10^{-9} S cm^{-1}, which are in the range of those values observed for **1**, **1**·S, **4**, and **5**.[9a,23]

Structural analysis can help to rationalize these conductivity values. Thus, the short Cu−Cu, Cu−I, and Cu−S distances (Table 1) and the chain angles (Tables S40−S62) are probably the key to understanding the electrical conductivity in these 1D and 2D CPs because they affect the electron delocalization taking place along the chains as a consequence of the copper (d_z) and halogen and sulfur (p_z) orbital overlap; i.e., a more effective overlap between these orbitals gives rise to better electrical conductivity, which typically imposes a shortening in the distances. As expected, the obtained values for **1**, **1**·THF, and **5** are ca. 1−2 orders of magnitude smaller than those obtained using micrometer crystals. This difference is due to the well-known effect of the intergrain contacts that increases the resistivity in the pellets.

Computed Density of Electronic States. For a deeper rationalization of the physical properties, theoretical calculations on these CPs were carried out. Figure 9 shows the computed density of electronic states (in arbitrary units) for the different compounds of the present study as a function of the energy referring to the Fermi level (in eV). Besides the total density of states, we have also computed the projected density of states (PDOS) onto the organic ligands, onto the metallic chains, and onto the functional groups THF, acetone, and MeOH. For all of these cases, theory predicts a canonical narrow-gap semiconducting character with electronic gaps ranging between 1.2 and 1.5 eV, where most of the compounds behave as n-type semiconductors (with the Fermi level almost

DOI: 10.1021/acs.inorgchem.8b03364
Inorg. Chem. XXXX, XXX, XXX−XXX

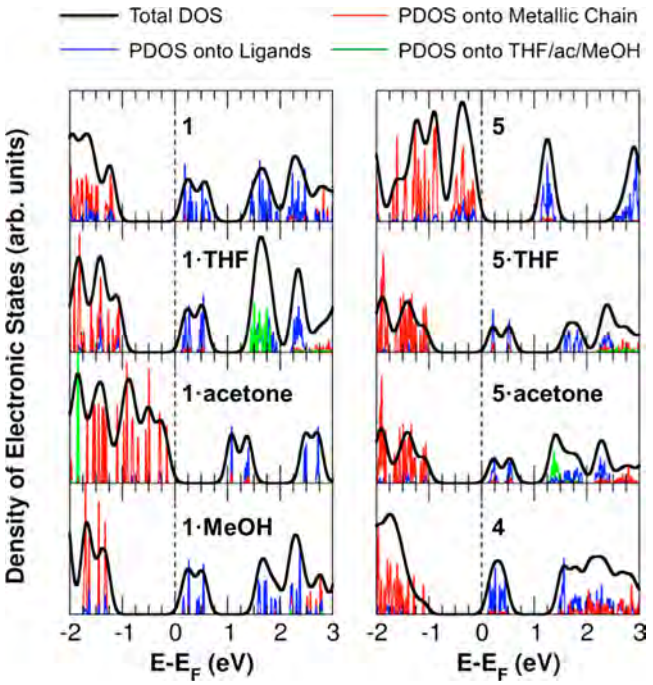

Figure 9. Computed total density of electronic states (in arbitrary units) for the different compounds as a function of the energy referring to the Fermi level (in eV), depicted by black lines. PDOS onto the organic ligands, onto the metallic chains, and onto the THF, acetone, and MeOH molecules depicted by blue, red, and green lines, respectively.

pinning the CB), except the **5** and **5**·acetone systems, which exhibit a p-type semiconducting character with the Fermi level pinning the VB.

It is interesting to notice that a fair correlation can be found between the computed band-gap values and the experimental conductivity ones (Table 2). Because the conductivity values increase across the different compounds, the computed CB−VB gaps decrease. Additionally, although all of the band-gap values lie in a very narrow window, a noticeable change is theoretically predicted between the **1**·acetone (1.22 eV) and **1**·MeOH (1.36 eV) compounds, with the latter being close to the case of compound **1**. On the other hand, it is also interesting how the band-gap values computed for **5**, **5**·THF, and **5**·acetone compounds are very close, ranging between 1.21 and 1.27 eV.

Additionally, because of the high structural symmetry of the compounds, the electronic degeneracy of the electronic states, close to the Fermi level, shows electronic multiplicity. Density of states profiles show remarkable similarities for all of the compounds. It is interesting to notice how the CB, and a set of close electronic states, yields in all cases one- or two-peak features. These electronic states will be of particular importance in the analysis of the optical properties, with the electronic states, together with the VB, being involved in the most important optical transitions within the experimental range of interest (450−750 nm).

Regarding the PDOS profiles for all cases, it is possible to observe, as expected in these kinds of compounds, that the VB is mostly formed by electronic states from the metallic chain, while the CB and its closest empty states are formed by electronic states located on the organic ligands. For those compounds incorporating THF, acetone, and MeOH from the synthesis, the electronic states associated with these functional groups locate far from the gap region, which will not have any influence on the optical properties beyond their structural influence in the crystal-cell relaxation. It is important to remark how, depending on each specific compound, induced electronic states of the metallic chains reflect in the CB region or induced electronic states of the organic ligands reflect in the VB. This observation is related with the overlapping degree between the valence and conduction states, which will have its reflection in the efficiency of the optical transitions between such states.

Excitation Spectra: TDDFT + CIS. Figure S56 shows the computed TDDFT photoexcitation spectra for the different compounds as a function of the photon wavelength (in nm) for structures resolved at two different temperatures for each compound at standard pressure. As a first observation, one realizes that all of the spectra, within the wavelength region of experimental interest (450−750 nm), show a two-peak feature, except **4**, which only exhibits a wide unique peak. The CIS method permits one to compute the contribution (in %) of an electronic transition between two electronic states to a given excitation energy. In Figure S56, we show the most important electronic transitions contributing to each excitation peak. Specifically, in this study, the CIS-based analysis permits one to assign to all the two-peak features two distinct and prominent transitions (>75% of contribution): a low-energy excitation corresponding to electronic transitions between the VB and CB (ranging between 620 and 635 nm at 110 K and between 630 and 650 nm at RT) and the high-energy excitation corresponding to electronic transitions between the VB to CB +1 (ranging between 560 and 580 nm at 110 K and between 565 and 595 nm at RT). As mentioned, for the case of **4**, just one wide peak is observed in this wavelength window because of the high electronic degeneracy of its CB comprising a large number of electronic states with very similar eigenenergies. For this system, the 110 K and RT peaks are located at 604 and 622 nm (corresponding to the VB → CB transition), respectively. Residual electronic transition contributions (<25%) to the main excitations correspond to transitions between electronic states close but deeper than the VB and CB/CB+1.

Interestingly, the photoexcitation intensity is more pronounced in all cases for the low-temperature structures. At this point, it is important to remark that the differences observed between the different compounds within our theoretical formalism are exclusively due to the structural differences; no environmental temperature effects, such as temperature-induced band broadening, can be captured by our approach beyond the reflection of temperature in the crystal structure. Nonetheless, the trend observed is consistent with the photoluminescence spectra and the associated photoelectronic decay. Besides, a slight shift toward lower photon energies is observed in all of the structures. This behavior may be explained in terms of the electronic states narrowing in the high-temperature structures in the electronic states close to the gap. Most intense average photoexcitation signal is obtained for the compounds involving iodine, including **4**. It is also worth noticing that the gap between the high- and low-energy excitations is slightly higher for these iodine-based compounds, for which the excitation intensity differences between the low- and high-temperature structures are also more pronounced. On the other hand, regarding Figure S56, theory predicts a lower TDDFT photoexcitation response for the compounds

DOI: 10.1021/acs.inorgchem.8b03364
Inorg. Chem. XXXX, XXX, XXX−XXX

involving bromine. This difference between the optical intensity in iodine- and bromine-based compounds may have its origin in the slight overlapping between the VB and CB. In Figure S56, for bromine-based compounds, it is possible to appreciate how some induced reflection of the metallic chain electronic states appear in the CB and vice versa. This slight overlapping between states with different electronic character (metallic/organic) could decrease the efficiency of the electronic transitions, reducing the photoexcitation intensity. This effect is also observable in the experiments.

As explained in a previous section, computed PDOS profiles of Figure S56 shows the VB mostly located at the metallic chains, while the CB and CB+1 are spatially located fundamentally in the organic ligands. Thus, the electronic origin of the transitions reported here is purely metallorganic (i.e., metal−ligand transitions). The 3D morphology and spatial distribution and location of the VB, CB, and CB+1 for all the compounds analyzed here can be found, as depicted in Figure S57. In this figure, the 3D orbital isodensities corresponding to the VB, CB, and CB+1 states are all represented by an isodensity value of 10^{-4} au.

To conclude, it is worth mentioning that, from theoretical analysis, the THF, acetone, and MeOH molecules present in some of the crystals do not seem to have any influence on the optical properties, which do not contribute electronically to the VB, CB, or CB+1 states (Figure S56), responsible of the most pronounced optical transitions. This evidence is also visible in Figure S57.

CONCLUSIONS

In summary, this work shows the high structural versatility of the structurally simple TBA ligands. In particular, it presents the results of direct reactions, under ambient conditions, of TBA and DTBA with CuX (X = I, Br). These reactions gave rise to multifunctional 1D and 2D CPs. The isolated 1D CPs **1** and **5** showed the ability to accommodate a variety of organic solvents located in their structures, leading to the solvated species **1**·S (S = THF, acetone, MeOH) and **5**·S (S = THF, acetone). Interestingly, the electronic properties, i.e., luminescence and electrical semiconductivity, of **1**·S or **5**·S are significantly different, allowing VOC detection. Thus, for instance, **1** is able to detect the presence of THF or acetone at RT but **5** only at low temperature. Theoretical calculations have been used to rationalize these findings.

This work paves new possibilities in terms of structural and material chemistry for the use of thioamide ligands.

ASSOCIATED CONTENT

Supporting Information

The Supporting Information is available free of charge on the ACS Publications website at DOI: 10.1021/acs.inorgchem.8b03364.

Additional experimental information, theoretical studies, and physical properties (PDF)

Accession Codes

CCDC 1835539−1835559 contain the supplementary crystallographic data for this paper. These data can be obtained free of charge via www.ccdc.cam.ac.uk/data_request/cif, or by emailing data_request@ccdc.cam.ac.uk, or by contacting The Cambridge Crystallographic Data Centre, 12 Union Road, Cambridge CB2 1EZ, UK; fax: +44 1223 336033.

AUTHOR INFORMATION

Corresponding Authors

*E-mail: felix.zamora@uam.es.

*E-mail: salome.delgado@uam.es.

ORCID

Josefina Perles: 0000-0003-0256-0186

Pilar Amo-Ochoa: 0000-0002-1952-1020

Vanesa Fernández-Moreira: 0000-0002-1218-7218

Félix Zamora: 0000-0001-7529-5120

Notes

The authors declare no competing financial interest.

ACKNOWLEDGMENTS

MINECO (Grants MAT2016-77608-C3-1-P, MAT2016-75883-C2-1-P, and MAT2017-85089-C2-1-R; Ramon y Cajal, Grant RYC-2015-17730), Ministerio de Ciencia, Innovación y Universidades (Grant CTQ2016-75816-C2-1-P), and European Union's Horizon 2020 research and innovation programme (Grant 785219; Graphene Flagship−core2).

REFERENCES

(1) Batten, S. R.; S. M. N, Turner, D. R. *Coordination Polymers: Design, Analysis and Application*; RSC Publishing, 2009.

(2) (a) Hassanein, K.; Conesa-Egea, J.; Delgado, S.; Castillo, O.; Benmansour, S.; Martínez, J.-I.; Abellán, G.; Gómez-García, C.-J. C.; Zamora, F.; Amo-Ochoa, P. Electrical Conductivity and Strong Luminescence in Copper Iodide Double Chains with Isonicotinato Derivatives. *Chem. - Eur. J.* **2015**, *21*, 17282−17292. (b) Amo-Ochoa, P.; Hassanein, K.; Gomez-Garcia, C. J.; Benmansour, S.; Perles, J.; Castillo, O.; Martinez, J. I.; Ocon, P.; Zamora, F. Reversible Stimulus-Responsive Cu(I) Iodide Pyridine Coordination Polymer. *Chem. Commun.* **2015**, *51*, 14306−14309. (c) Delgado, S.; Sanz Miguel, P. J.; Priego, J. L.; Jiménez-Aparicio, R.; Gómez-García, C. J.; Zamora, F. A Conducting Coordination Polymer Based on Assembled Cu9 Cages. *Inorg. Chem.* **2008**, *47*, 9128−9130. (d) Gallego, A.; Castillo, O.; Gómez-García, C. J.; Zamora, F.; Delgado, S. Electrical Conductivity and Luminescence in Coordination Polymers Based on Copper(I)-Halides and Sulfur-Pyrimidine Ligands. *Inorg. Chem.* **2012**, *51*, 718−727.

(3) (a) Ford, P. C.; Cariati, E.; Bourassa, J. Photoluminescence Properties of Multinuclear Copper(I) Compounds. *Chem. Rev.* **1999**, *99*, 3625−3648. (b) Yam, V. W.-W.; Lo, K. K.-W. Luminescent Polynuclear D10 Metal Complexes. *Chem. Soc. Rev.* **1999**, *28* (5), 323−334.

(4) (a) Blake, A. J.; Champness, N. R.; Hubberstey, P.; Li, W.-S.; Withersby, M. A.; Schröder, M. Inorganic Crystal Engineering Using Self-Assembly of Tailored Building-Blocks. *Coord. Chem. Rev.* **1999**, *183*, 117−138. (b) Peng, R.; Li, M.; Li, D. Copper(I) Halides: A Versatile Family in Coordination Chemistry and Crystal Engineering. *Coord. Chem. Rev.* **2010**, *254*, 1−18. (c) Graham, P. M.; Pike, R. D.; Sabat, M.; Bailey, R. D.; Pennington, W. T. Coordination Polymers of Copper(I) Halides. *Inorg. Chem.* **2000**, *39*, 5121−5132.

(5) (a) Cariati, E.; Lucenti, E.; Botta, C.; Giovanella, U.; Marinotto, D.; Righetto, S. Cu(I) Hybrid Inorganic−Organic Materials with Intriguing Stimuli Responsive and Optoelectronic Properties. *Coord. Chem. Rev.* **2016**, *306*, 566−614. (b) Tsuge, K.; Chishina, Y.; Hashiguchi, H.; Sasaki, Y.; Kato, M.; Ishizaka, S.; Kitamura, N. Luminescent Copper(I) Complexes with Halogenido-Bridged Dimeric Core. *Coord. Chem. Rev.* **2016**, *306*, 636−651. (c) Li, J.-C.; Li, H.-X.; Li, H.-Y.; Gong, W.-J.; Lang, J.-P. Ligand Coordination Site-Directed Assembly of Copper(I) Iodide Complexes of ((Pyridyl)-1-pyrazolyl)pyridine. *Cryst. Growth Des.* **2016**, *16*, 1617−1625.

(6) (a) Zhu, H.-B.; Gou, S.-H. In Situ Construction of Metal−Organic Sulfur-Containing Heterocycle Frameworks. *Coord. Chem.*

DOI: 10.1021/acs.inorgchem.8b03364
Inorg. Chem. XXXX, XXX, XXX−XXX

Rev. **2011**, *255*, 318−338. (b) Yang, X.-J.; Li, H.-X.; Xu, Z.-L.; Li, H.-Y.; Ren, Z.-G.; Lang, J.-P. Spacer length-controlled assembly of [CunIn]-based coordination polymers from CuI and bis(4-phenylpyrimidine-2-thio)alkane ligands. *CrystEngComm* **2012**, *14*, 1641−1652. (c) Li, H.-X.; Zhao, W.; Li, H.-Y.; Xu, Z.-L.; Wang, W.-X.; Lang, J.-P. [Cu30I16(mtpmt)12(μ10-S4)]: an unusual 30-membered copper(i) cluster derived from the C−S bond cleavage and its use in heterogeneous catalysis. *Chem. Commun.* **2013**, *49*, 4259−426.

(7) Lobana, T. S.; Sharma, R.; Bawa, G.; Khanna, S. Bonding and Structure Trends of Thiosemicarbazone Derivatives of Metals—an Overview. *Coord. Chem. Rev.* **2009**, *253*, 977−1055.

(8) (a) Mes, T.; Cantekin, S.; Balkenende, D. W. R.; Frissen, M. M. M.; Gillissen, M. A. J.; De Waal, B. F. M.; Voets, I. K.; Meijer, E. W.; Palmans, A. R. A. Thioamides: Versatile Bonds to Induce Directional and Cooperative Hydrogen Bonding in Supramolecular Polymers. *Chem. - Eur. J.* **2013**, *19*, 8642−8649. (b) Eccles, K. S.; Morrison, R. E.; Maguire, A. R.; Lawrence, S. E. Crystal Landscape of Primary Aromatic Thioamides. *Cryst. Growth Des.* **2014**, *14*, 2753−2762. (c) Lytvynenko, A. S.; Kolotilov, S. V.; Cador, O.; Golhen, S.; Ouahab, L.; Pavlishchuk, V. V. Antiferromagnetic Ordering in Cobalt(Ii) and Nickel(Ii) 1d Coordination Polymers with the Dithioamide of 1,3-Benzenedicarboxylic Acid. *New J. Chem.* **2011**, *35*, 2179−2186.

(9) (a) Troyano, J.; Perles, J.; Amo-Ochoa, P.; Martinez, J. I.; Zamora, F.; Delgado, S. Reversible Recrystallization Process of Copper and Silver Thioacetamide-Halide Coordination Polymers and Their Basic Building Blocks. *CrystEngComm* **2014**, *16*, 8224−8231. (b) Troyano, J.; Perles, J.; Amo-Ochoa, P.; Zamora, F.; Delgado, S. Strong Luminescent Copper(I) Halide Coordination Polymers and Dinuclear Complexes with Thioacetamide and N,N[Prime or Minute]-Donor Ligands. *CrystEngComm* **2016**, *18*, 1809−1817. (c) Troyano, J.; Castillo, O.; Martínez, J. I.; Fernández-Moreira, V.; Ballesteros, Y.; Maspoch, D.; Zamora, F.; Delgado, S. Reversible Thermochromic Polymeric Thin Films Made of Ultrathin 2d Crystals of Coordination Polymers Based on Copper(I)-Thiophenolates. *Adv. Funct. Mater.* **2018**, *28*, 1704040.

(10) Dixon, S.; Whitby, R. J. Efficient Synthesis of Thioamide Terminated Molecular Wires. *Tetrahedron Lett.* **2006**, *47*, 8147−8150.

(11) (a) Gonze, X. Adiabatic Density-Functional Perturbation Theory. *Phys. Rev. A: At., Mol., Opt. Phys.* **1995**, *52*, 1096−1114. (b) Baroni, S.; Giannozzi, P.; Testa, A. Green's-Function Approach to Linear Response in Solids. *Phys. Rev. Lett.* **1987**, *58*, 1861−1864. (c) Baroni, S.; de Gironcoli, S.; Dal Corso, A.; Giannozzi, P. Phonons and Related Crystal Properties from Density-Functional Perturbation Theory. *Rev. Mod. Phys.* **2001**, *73*, 515−562. (d) Rocca, D.; Gebauer, R.; Saad, Y.; Baroni, S. Turbo Charging Time-Dependent Density-Functional Theory with Lanczos Chains. *J. Chem. Phys.* **2008**, *128*, 154105. (e) Walker, B.; Gebauer, R. Ultrasoft Pseudopotentials in Time-Dependent Density-Functional Theory. *J. Chem. Phys.* **2007**, *127*, 164106. (f) Walker, B.; Saitta, A. M.; Gebauer, R.; Baroni, S. Efficient Approach to Time-Dependent Density-Functional Perturbation Theory for Optical Spectroscopy. *Phys. Rev. Lett.* **2006**, *96*, 113001.

(12) Monkhorst, H. J.; Pack, J. D. Special Points for Brillouin-Zone Integrations. *Phys. Rev. B* **1976**, *13*, 5188−5192.

(13) Perdew, J. P.; Burke, K.; Ernzerhof, M. Generalized Gradient Approximation Made Simple. *Phys. Rev. Lett.* **1996**, *77*, 3865−3868.

(14) Vanderbilt, D. Soft Self-Consistent Pseudopotentials in a Generalized Eigenvalue Formalism. *Phys. Rev. B: Condens. Matter Mater. Phys.* **1990**, *41*, 7892−7895.

(15) Frisch, M. J.; Trucks, G. W.; Schlegel, H. B.; Scuseria, G. E.; Robb, M. A.; Cheeseman, J. R.; Scalmani, G.; Barone, V.; Petersson, G. A.; Nakatsuji, H.; Li, X.; Caricato, M.; Marenich, A. V.; Bloino, J.; Janesko, B. G.; Gomperts, R.; Mennucci, B.; Hratchian, H. P.; Ortiz, J. V.; Izmaylov, A. F.; Sonnenberg, J. L.; Williams; Ding, F.; Lipparini, F.; Egidi, F.; Goings, J.; Peng, B.; Petrone, A.; Henderson, T.; Ranasinghe, D.; Zakrzewski, V. G.; Gao, J.; Rega, N.; Zheng, G.; Liang, W.; Hada, M.; Ehara, M.; Toyota, K.; Fukuda, R.; Hasegawa, J.; Ishida, M.; Nakajima, T.; Honda, Y.; Kitao, O.; Nakai, H.; Vreven, T.; Throssell, K.; Montgomery, J. A., Jr.; Peralta, J. E.; Ogliaro, F.; Bearpark, M. J.; Heyd, J. J.; Brothers, E. N.; Kudin, K. N.; Staroverov, V. N.; Keith, T. A.; Kobayashi, R.; Normand, J.; Raghavachari, K.; Rendell, A. P.; Burant, J. C.; Iyengar, S. S.; Tomasi, J.; Cossi, M.; Millam, J. M.; Klene, M.; Adamo, C.; Cammi, R.; Ochterski, J. W.; Martin, R. L.; Morokuma, K.; Farkas, O.; Foresman, J. B.; Fox, D. J. *Gaussian16*, revision B.01; Gaussian Inc.: Wallingford, CT, 2016.

(16) Foresman, J. B.; Head-Gordon, M.; Pople, J. A.; Frisch, M. J. Toward a Systematic Molecular Orbital Theory for Excited States. *J. Phys. Chem.* **1992**, *96*, 135−149.

(17) Lenstra, A. T. H.; Tavernier, S.; Versichel, W. Crystal Structure of Cuprous Chloride Tri-thiobenzamide. *Bull. Soc. Chim. Belg.* **1977**, *86*, 419.

(18) (a) Cariati, E.; Bu, X.; Ford, P. C. Solvent- and Vapor-Induced Isomerization between the Luminescent Solids [Cui(4-Pic)]4 and [Cui(4-Pic)]∞ (Pic = Methylpyridine). The Structural Basis for the Observed Luminescence Vapochromism. *Chem. Mater.* **2000**, *12*, 3385−3391. (b) Ciurtin, D. M.; Pschirer, N. G.; Smith, M. D.; Bunz, U. H. F.; zur Loye, H.-C. Two Luminescent Coordination Polymers with a Triple-Helix Structure: Hgx2(C31h24n2)·Ch2cl2 (X = Cl and Br). *Chem. Mater.* **2001**, *13*, 2743−2745. (c) Wurthner, F.; Sautter, A. Highly Fluorescent and Electroactive Molecular Squares Containing Perylene Bisimide Ligands. *Chem. Commun.* **2000**, 445−446.

(19) (a) Habib, H. A.; Hoffmann, A.; Höppe, H. A.; Steinfeld, G.; Janiak, C. Crystal Structure Solid-State Cross Polarization Magic Angle Spinning 13c Nmr Correlation in Luminescent D10 Metal-Organic Frameworks Constructed with the 1,2-Bis(1,2,4-Triazol-4-Yl)Ethane Ligand. *Inorg. Chem.* **2009**, *48*, 2166−2180. (b) Yam, V. W.-W.; Wong, K. M.-C. Luminescent Metal Complexes of D6, D8 and D10 Transition Metal Centres. *Chem. Commun.* **2011**, *47*, 11579−11592.

(20) (a) Vega, A.; Saillard, J.-Y. Bonding in Tetrahedral Cu4(M3-X)4l4 Copper(I) Clusters: A Dft Investigation. *Inorg. Chem.* **2004**, *43*, 4012−4018. (b) De Angelis, F.; Fantacci, S.; Sgamellotti, A.; Cariati, E.; Ugo, R.; Ford, P. C. Electronic Transitions Involved in the Absorption Spectrum and Dual Luminescence of Tetranuclear Cubane [Cu4i4(Pyridine)4] Cluster: A Density Functional Theory/Time-Dependent Density Functional Theory Investigation. *Inorg. Chem.* **2006**, *45*, 10576−10584. (c) Perruchas, S.; Tard, C.; Le Goff, X. F.; Fargues, A.; Garcia, A.; Kahlal, S.; Saillard, J.-Y.; Gacoin, T.; Boilot, J.-P. Thermochromic Luminescence of Copper Iodide Clusters: The Case of Phosphine Ligands. *Inorg. Chem.* **2011**, *50* (21), 10682−10692. (d) Henline, K. M.; Wang, C.; Pike, R. D.; Ahern, J. C.; Sousa, B.; Patterson, H. H.; Kerr, A. T.; Cahill, C. L. Structure, Dynamics, and Photophysics in the Copper(I) Iodide−Tetrahydrothiophene System. *Cryst. Growth Des.* **2014**, *14*, 1449−1458. (e) Liu, Z.; Djurovich, P. I.; Whited, M. T.; Thompson, M. E. Cu4i4 Clusters Supported by P∧N-Type Ligands: New Structures with Tunable Emission Colors. *Inorg. Chem.* **2012**, *51*, 230−236.

(21) Zink, D. M.; Volz, D.; Baumann, T.; Mydlak, M.; Flügge, H.; Friedrichs, J.; Nieger, M.; Bräse, S. Heteroleptic, Dinuclear Copper(I) Complexes for Application in Organic Light-Emitting Diodes. *Chem. Mater.* **2013**, *25*, 4471−4486.

(22) Givaja, G.; Amo-Ochoa, P.; Gomez-Garcia, C. J.; Zamora, F. Electrical Conductive Coordination Polymers. *Chem. Soc. Rev.* **2012**, *41*, 115−147.

(23) Troyano, J.; Perles, J.; Amo-Ochoa, P.; Martínez, J. I.; Concepción Gimeno, M.; Fernández-Moreira, V.; Zamora, F.; Delgado, S. Luminescent Thermochromism of 2d Coordination Polymers Based on Copper(I) Halides with 4-Hydroxythiophenol. *Chem. - Eur. J.* **2016**, *22*, 18027−18035.

DOI: 10.1021/acs.inorgchem.8b03364
Inorg. Chem. XXXX, XXX, XXX−XXX